A Cohesive Zone Model approach to interlaminar behaviour of carbon/epoxy laminated curved beams

David Ranz[a,*], Jesus Cuartero[b], Luis Castejon[b], Ramon Miralbes[a], Hugo Malon[b]
[a.] Departamento de Diseño y Fabricación, Universidad de Zaragoza, Zaragoza, Spain
[b.] Departamento de Ingeniería Mecánica, Universidad de Zaragoza, Zaragoza, Spain

Abstract

This study analytically investigates the behaviour of carbon/epoxy laminated curved beams subjected to interlaminar tensile stress by means of a four-point-bending test, carried out in compliance with ASTM D6415 Standard. A Cohesive Zone Model (CZM) has been used to analyse the interlaminar tensile strength (ILTS) and the post-failure behaviour for lay-ups in several thicknesses, as well as the location of first and subsequent predicted delamination. In this study, the model behaviour is described by a bilinear constitutive model. Initially, a law of traction-separation governs the elastic behaviour, until satisfying a quadratic criterion that establishes the failure and degradation starting at the interface. Finally, a law describes the evolution of the damage and the interaction in mixed-mode conditions, which leads to the final failure of the interface and delamination onset. Two-dimensional finite element models (FEM) have been created to apply the CZM and analyse the influence of several cohesive model parameters, such as, cohesive element stiffness, cohesive element size and critical energy release rate. Predicted load-displacement curves have been compared with the experimental results obtained and strong correlation has been observed. The ILTS values predicted by the two-dimensional models show deviations no greater than 5.6% in comparison with the experimental results. These models and the influence of their parameters play an important role in the prediction of the interlaminar tensile strength and the post-failure behaviour of laminated curved beams.

Keywords
Interlaminar tensile strength; Cohesive elements; Delamination; Four-point-bending; Laminated curved beam

1. Introduction.

Components made of composite materials, incorporating zones of important bending radius are commonly present in a wide range of engineering structures, such as those found in aeronautics, the maritime industry and energy or civil construction [1]. The main failure that takes place in these components results from poor Interlaminar Tensile Strength (ILTS) properties of the materials used, leading to delamination between layers [2], [3]. Thus, determining ILTS and its post-failure evolution is key when approaching the development of efficient designs. As Ranz et al [4] show, there are several experimental methodologies available to determine ILTS. In this study an indirect load methodology – a four point bending test in accordance with ASTM D6415 Standard – is simulated [5] to predict interlaminar behaviour. Numerical methodologies to predict ILTS in curved beams are proposed in several

* Corresponding author. E-mail address: dranz@unizar.es

studies, such as those carried out by Avalon [6], Raju [2], Ross [7] and Nguyen [8]. Chiefly, two numerical methodologies to tackle this problem are currently implemented in the finite elements packages: Virtual Crack Closure Technique (VCCT) [9]–[12] and Cohesive Zone Model (CZM) [2], [13]–[17], the latter in two different versions, one using cohesive surfaces and the other using interface elements, also called cohesive elements. CZM models are considered quite efficient when interface strength is low when compared to the surrounding area's interface strength. That is the situation when talking about composite materials´ laminates [18].
The case considered in the current paper does not have initial damage pointing to a location where delamination could occur. Regardless of such lack of initial damage, it is well known that delamination will occur through some interface planes of the stacking sequence. Therefore, CZM methodology was selected to develop the numerical methods. In addition, cohesive elements were used in the method applied, instead of those methods that apply cohesive surfaces. Despite greater preprocessing effort being required when applying cohesive elements, they were selected due to the better control achieved for mesh density and interface stiffness. Moreover, the selected software suite was ABAQUS [19], an extremely powerful general open Finite Element Method software, which allows the key aspect of selecting multiple and simultaneous failure mechanisms occurring during delamination.
The constitutive law for the traction-separation curve for the cohesive elements is the bilinear curve stated by Alfano [20]. This type of curve is considered as the best option based upon a balance between result accuracy and computational cost.
This bilinear law will govern delamination evolution and is defined by the following characteristics [15][21], [22]: First, there is an initial elastic part having high interface stiffness (K), which is maintained until the maximum interlaminar strength is reached (T_o). After such a peak, a softening behaviour takes place until the stress is equal to zero. The area below the force-displacement curve is equal to the interlaminar fracture strength (G_c). Whenever a cohesive element reaches the maximum interlaminar strength, failure initiates; and when the area below the curve equals G_c, the cohesive element fails and the delamination propagates.

The need for accurate results, the difficulty of convergence in some instances and the need to apply a fine mesh [23] leads to high computational time for calculation. 2D models were used for this reason. These 2D models allow for performing the sensitivity analysis of the different parameters involved in the cohesive model definition. Models were calculated with ABAQUS [19], including an extensive library of 3D, 2D and axisymmetric cohesive elements. In addition, ABAQUS allows the selection and adjustment of different criteria to determine failure onset and damage evolution, as well as the possibility of defining the relationship between mixed failure modes.

Finally, the predicted results of ILTS and post-failure evolution are correlated with the experimental results presented by Ranz et al [4] in unidirectional (UD) 4,8,12 carbon / epoxy layered laminated curved test coupons.

2. Cohesive Zone Model description

The fact that the paper is focused on a unidirectional lay-up in which an initial elastic response of the material is expected, the traction-separation model is considered to be the best choice in order to determine cohesive behaviour [20]. Such elastic behaviour can be modelled through a matrix linking both nominal stress and nominal strains in the interface. These nominal stresses are calculated from each one of the force components divided by the initial area of the interface,

whereas nominal strains are calculated from the existing separation divided by the initial thickness.

Nominal stress vector in the interface, t, consists of three components in the case of 3D models and two components in the case of 2D models. There is always one component representing the normal traction of the interface. However, the other two stress components are related to shear tractions, while there is only one shear traction for 2D models.

Nominal strains are defined as follows:

$$\varepsilon_n = \frac{\delta_n}{t_o};\ \varepsilon_s = \frac{\delta_s}{t_o};\ \varepsilon_t = \frac{\delta_t}{t_o}, \tag{1}$$

Where separations in each direction are named as d_n, d_s y d_t; and original thickness is t_o. Therefore the elastic behaviour can be defined as:

$$T = \begin{Bmatrix} T_n \\ T_s \\ T_t \end{Bmatrix} = \begin{bmatrix} K_{nn} & K_{ns} & K_{nt} \\ K_{ns} & K_{ss} & K_{st} \\ K_{nt} & K_{st} & K_{tt} \end{bmatrix} \begin{Bmatrix} \varepsilon_n \\ \varepsilon_s \\ \varepsilon_t \end{Bmatrix} \tag{2}$$

The initial response of the model is considered fully linear until the condition defined by the damage criterion is met.

The damage criterion is based on a quadratic stress criterion applied on the interface, as described by Ye [24] and Brewer [25]. This criterion states damage onset at the interface, that it is to say, degradation starts at a specific point. Moreover, it shows strong correlation with stress values when delamination failure starts.

Such criterion states damage onset when the criterion is set to 1. The criterion is a quadratic interaction involving out-of-plane interlaminar stresses and the corresponding strength values.

$$\left(\frac{\langle T_n \rangle}{T_n^o}\right)^2 + \left(\frac{T_s}{T_s^o}\right)^2 + \left(\frac{T_t}{T_t^o}\right)^2 = 1 \tag{3}$$

T_n^o, T_s^o and T_t^o represent maximum interlaminar strengths out of the plane, when strain is normal to the interface, or in both shear directions, respectively. Symbol $\langle\ \rangle$ represents Macaulay brackets, indicating that, under compressive stresses, damage is not initiated.

Damage evolution describes how interface stiffness is degraded once the damage criterion limit is met. D variable states global material damage and involves the combined effect of all active mechanisms operating in the model. At the beginning, when the interface is intact, damage variable D is set to 0 and evolves linearly until its maximum value is equal to one, following the cohesive law shown in Figure 1. Stress components in the traction-separation model are affected by the damage as the following equations show:

$$T_n = \begin{cases} (1-D)\overline{T}_n; & \overline{T}_n \geq 0 \\ \overline{T}_n;\ (no\ damage\ under\ stress) \end{cases}$$

$$\left.\begin{aligned} T_s &= (1-D)\overline{T}_s \\ T_t &= (1-D)\overline{T}_t \end{aligned}\right| \quad with\ T_{shear} = T_s + T_t \tag{4}$$

Where $\overline{T}_n$, $\overline{T}_s$ y $\overline{T}_t$ are the stress components from the traction-separation law if failure has not happened, which can be obtained from eq (2).

Researchers Camanho and Davila [21] recommended using effective displacement in order to show damage evolution under a combination of normal and shear strains at the interface.

$$\delta_m = \sqrt{\langle \delta_n \rangle^2 + \delta_s^2 + \delta_t^2} \tag{5}$$

Damage evolution in the present model is governed by the energy released throughout the whole damage process, that is to say, fracture energy. This energy is represented in the area below the traction-separation curve. The relationships of such energy to the mixed mode are governed by the fracture criterion proposed by Benzeggagh and Kenane [26], which is shown in (6):

$$G_{IC} + (G_{IIC} - G_{IC}) \left(\frac{G_{shear}}{G_T}\right)^{\eta} = G_C; \quad with \quad G_T = G_I + G_{shear} \quad y \quad G_{shear} = G_{II} + G_{III} \tag{6}$$

Where η is a material parameter set to a value of 2.284 for carbon fiber-epoxy UD laminates. Such figure was determined by successful researches [21], [27], [28]. Variable D, is the damage evolution variable, and equation (7) shows its value for a linear softening law, as the one showed in Figure 1. D is defined as a relationship between the displacement jumps.

$$\begin{cases} D = 0; \quad if \quad \delta_m^{max} < \delta_m^o \\ D = \frac{\delta_m^f (\delta_m^{max} - \delta_m^o)}{\delta_m^{max} \left(\delta_m^f - \delta_m^o\right)}; \quad if \ \delta_m^o < \delta_m^{max} < \delta_m^f \\ D = 1; \quad if \quad \delta_m^f < \delta_m^{max} \end{cases} \tag{7}$$

Where:

$$\delta_m^f = \frac{2G_C}{T_{eff}^o} \tag{8}$$

Softening law T_{eff}^o is the effective traction at the beginning of damage, and δ_m^{max} is the peak value of displacement during the load case.

The constitutive bilinear model for mixed- fracture mode is shown graphically in Figure 1. Fracture energy evolution is shown for mixed modes involving mode I and shear modes (II and III). Normal mode I and shear modes are represented in the vertical planes formed by the coordinate axes.

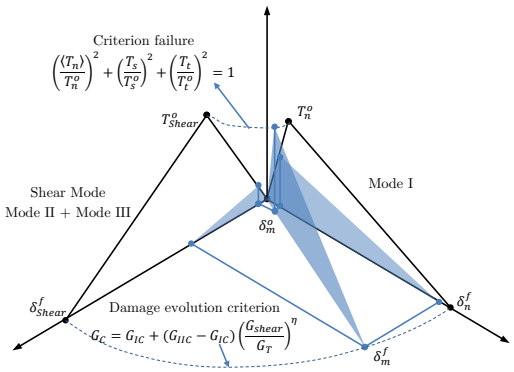

Figure 1. Bilinear constitutive model for mixed modes involving mode I and shear modes.

3. Finite Element Models

The dimensions of the Finite Element Model (FEM) are shown in Figure 2 (left). ASTM D6415 Standard was selected in order to perform the analysis. Models were developed in order to be compared with experimental studies previously carried out [4]. To achieve this goal, models for 4, 8 and 12 layer coupons were meshed and calculated.

High-density mesh was applied to the curved zone since the well-known delamination phenomenon occurs in such zone. Delamination starts and propagates from the curved zone; therefore, high-quality mesh density is needed in such zone. Such high-density mesh is spread until the area under the rollers is reached. Beyond the rollers, where supporting boundaries are set, mesh density is decreased in order to minimize computational cost. Layers are discretized in continuum solid elements [19]. Furthermore, all layers are connected to each other by means of cohesive elements simulating the interface between them. There are multiple connecting strategies in order to join cohesive and continuum elements when setting up the model. However, in the current study the selected strategy consisted in creating coincident nodes between interface and continuum element. Once cohesive elements are fully degraded, such elements are removed from calculation. This prevents any unwanted interference leading to result deviations.

Load rollers were set to a constant speed of 0.5 mm/min, whereas displacement on support rollers was restricted, as stated in the ASTM Standard [5]. Support rollers are allowed to rotate. Friction is almost negligible between the rollers and the carbon specimen.

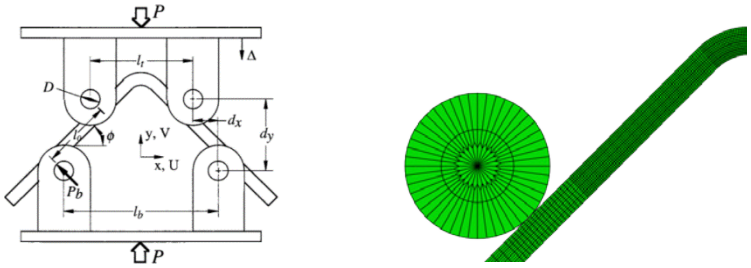

Figure 2. left) ASTM D6415 Test set-up; right) Detail of half 2D Finite Element Model (8 layers).

2D models were developed in the first adjustment stage in order to perform an analysis of parameter sensitivity focusing on the bilinear constitutive model parameters. Abaqus® software CPE4I elements were used for 2D models. These elements are linear plane strain elements with incompatibility mode control. Delamination onset and its propagation can be predicted by means of such elements due to their capacity to calculate interlaminar stresses through the thickness in a 2D model, whereas the interface was modelled with cohesive COH2D4 linear elements. These kinds of elements are included in ABAQUS element library.
Whenever a CZM model is applied to a finite element model, the definition of the properties of material must be entered in two sets: laminate material properties (Table 1); fracture constituent model properties of the cohesive surface (Table 2).
This approach allows us to determine failure onset, location and evolution. UD carbon-epoxy properties were collected from experimental testing. Plane test coupons were cut out from the laminates manufactured by means of resin infusion process, exactly the same process applied to the production of curved coupons [4]. It was impossible to evaluate some properties by

means of testing. In such situation, an asterisk (*) appears next to the corresponding figure. Those values not tested were estimated take into account the UD carbon-epoxy materials´ orthotropic behaviour.

Table 1. Properties of UD carbon-epoxy.

Elastic Properties						Strength Properties					
E_1 (GPa)	122	G_{12} (GPa)	4.4	ν_{12}	0.36	X_t (MPa)	1457	ε_1 (%)	1.28	S_{12} (MPa)	51.8
E_2 (GPa)	8.9	G_{13} (GPa)	4.4	ν_{13}*	0.18	Y_t (MPa)	28.5	ε_2 (%)	0.36	γ_{12} (%)	2.97
E_3 (GPa)*	8.9	G_{23} (GPa)	3.2	ν_{23}*	0.36	X_c (MPa)	775.3	ε_{1c} (%)	0.67	S_{13} (MPa)	51.2
Fiber volume V_f (%)	56					Y_c (MPa)	113.6	ε_{2c} (%)	2.01	S_{23} (MPa)*	51.2

Interface properties shown in Table 2 were collected from [15], [20], [29] , from very similar laminates, and later on, evaluated in the sensitivity analysis in order to select the appropriate properties for the present study.

Many authors [15], [20], [29] show the same values for interface stiffness (K), independently of the direction of traction on the interface. However, different values for both normal (n) and shear (s, t) stresses were applied in this study. In fact, some authors such as Yang [13] state that the same cohesive law is appropriate for both mode II and III.

Table 2. Interface properties.

Interface stiffness (N/mm^3)		Interface strength (N/mm^2)		Critical energy release rate (N/mm)	
K_n	4.6×10^5	T_n^o	45	G_{IC}	0.45
K_s	2.3×10^5	T_s^o	51	G_{IIC}	1.0
K_t	2.3×10^5	T_t^o	51	G_{IIIC}	1.0

4. Numerical and geometrical parameters' influence.

There are two mandatory conditions to meet in order to perform successful simulations by means of CZM. First, cohesive elements´ strain contribution to global strain must be quite low [30] in order to avoid an artificial deformation of the model. Second, cohesive element size must be smaller than cohesive zone length [29], [30]. These parameters and some others related to the cohesive bilinear law were analyzed in order to determine their validity and their influence when they are applied to curved specimens like those analyzed here. All these parameters were evaluated by means of a 12-layer numerical model, including 3 elements by layer through the thickness and 48 elements along the curved zone.

4.1. Effect of the cohesive element stiffness on the CZM

Cohesive stiffness is key to obtaining proper performance of a finite element model based on cohesive behaviour. There are different approaches to that problem. For example, Daudeville [31] calculates cohesive stiffness as a function of the thickness and the elastic modulus of the interface (resin-rich layer). Nevertheless, this hypothesis usually leads to high interface stiffness. Some authors such as Zou [32] propose using interface stiffness between 10^5 and 10^7 times the interface strength value divided by unit of length. Camanho [28] uses a value of about 10^6 N/mm^3 with no correction due to layers' thickness. However, Turon's approach [23] seems

to be more sensible, because of considerations about the mechanical behaviour of the laminate. High values of interface stiffness can lead to numerical problems, but this stiffness cannot be so low as to decrease the global stiffness of the model [32]. The 2D model was used to benchmark the influence of interface stiffness from 10^3 to 10^8 N/mm^3. Figure 3 charts show normalized load versus displacement. Below an interface stiffness value of 10^4 N/mm^3, the chart shows deviations from the expected behaviour pattern of the model. Under those circumstances, the model shows low global laminate stiffness, and calculations even stall or terminate prematurely because of convergence issues. In addition, for interface stiffness values between 10^4 and 10^7 N/mm^3 a similar model behaviour was obtained, with minimal deviations in terms of maximum loads reached, displacement at breakage and post-failure behaviour. However, interface stiffness of 10^8 N/mm^3 is too stiff and also leads to an earlier termination of post-delamination calculations, due to numerical problems.

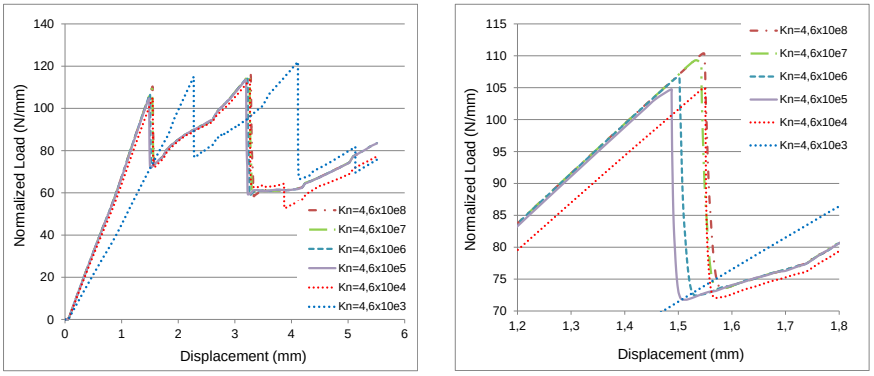

Figure 3. Interface stiffness effect. Delamination load detail (right).

The effects of stiffness in DCB tests for carbon-epoxy UD laminates was extensively researched by Zou [32]. Zou stated that load peak at which failure happens is overestimated if K_n/K_s is greater than 10. Furthermore, delamination onset is delayed under the same condition of K_n/K_s being greater than 10. However, delamination evolution usually works for K_n/K_s ratios around or below 1.

Most researchers [23], [33]–[35] applied the same interface stiffness values to their cohesive models for all directions, $K = K_n = K_s = K_t$, showing satisfactory results. The current study has set the rate K_n/K_s to 2 (Table 2). This value was selected after extensive calculations in which K_n/K_s ranged between 0.5 and 10. Results are presented, in Figure 4, with quite an accurate prediction for both stiffness and maximum peak load. Moreover, it was proven that the higher the ratio K_n/K_s, the faster the load recovers.

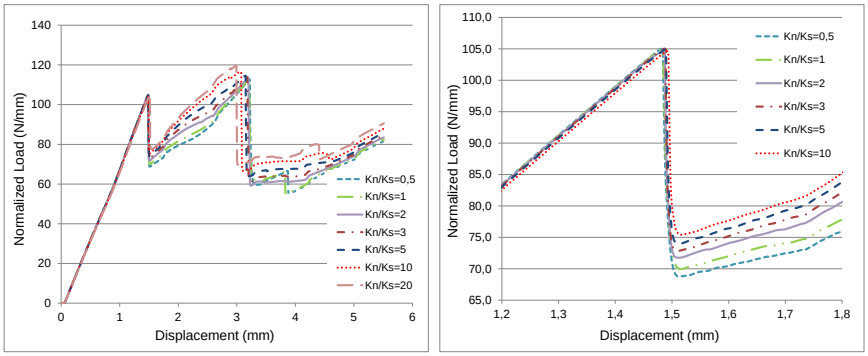

Figure 4. Influence of the interface stiffness ratio (K_n/K_s). Delamination load detail (right).

4.2. Characteristic length of the cohesive element in the CZM

The cohesive zone length is defined as the length where permanent damage occurs. Such damage usually occurs just on the tip of the crack. Precise results on delamination need a mesh fine enough to ensure that there is a minimum number of cohesive elements along the zone where the crack tip is formed [13], [23], [34], [36]. However, an extremely high number of elements could lead to both numerical issues and unaffordable computational cost. Therefore, a compromise between result accuracy and model complexity has to be found. Hilleborg [37] was a pioneer in the use of the CZM by using FEM for crack onset analysis and its evolution. He defined a characteristic length parameter (l_{ch}) for isotropic materials, exclusively dependent on material properties, which was stablished as follows:

$$l_{ch} = E\frac{G_c}{(\sigma_{max})^2} \tag{9}$$

In the case of crack growth occurring on orthotropic composite materials, Turon [23] adapted expression (9) for laminates, taking into account fracture modes I and II:

$$l_{ch,I} = ME_3\frac{G_{Ic}}{(T_n^o)^2} \tag{10}$$

$$l_{ch,II} = MG_{13}\frac{G_{IIc}}{(T_s^o)^2} \tag{11}$$

Where E_3 is the out-of-plane Young´s modulus, G_{13} is shear modulus in *13* plane (sliding plane), T_n^o y T_s^o are interface tensile and shear strength respectively. *M* is a parameter depending upon each CZM. Most common *M* values are those proposed by Hilleborg [37] and Rice [38] and both suggested the use of figures around 1. Nevertheless, Yang and Cox [13] considered expression (9) by replacing elastic moduli E_I and E_{II} by expressions (12) and (13) depending on the different material moduli and Poisson´s ratio of the orthotropic material.

$$\frac{1}{E_I} = \sqrt{\frac{b_{11}b_{33}}{2}}\sqrt{\left(\frac{b_{33}}{b_{11}}\right)^{1/2} + \frac{2b_{31}+b_{55}}{2b_{11}}} \tag{12}$$

$$\frac{1}{E_{II}} = \sqrt{\frac{b_{11}}{2}}\sqrt{(b_{11}b_{33})^{1/2} + \left(b_{31} + \frac{b_{55}}{2}\right)} \tag{13}$$

Where:

$$\begin{array}{lll} b_{11} = 1/E_{11}; & b_{12} = -\nu_{12}/E_{11}; & b_{66} = 1/G_{12}; \\ b_{22} = 1/E_{22}; & b_{23} = -\nu_{23}/E_{22}; & b_{55} = 1/G_{31}; \\ b_{33} = 1/E_{33}; & b_{31} = -\nu_{31}/E_{33}; & b_{44} = 1/G_{23}; \end{array}$$

Bao and Suo [39] stated an expression for the characteristic length in slim layers for Mode I as follows. This parameter for mode I depends exclusively on material properties:

$$l_{ch,I,slim} = \left[E_I\frac{G_{Ic}}{(T_n^o)^2}\right]^{1/4} t^{3/4} \tag{14}$$

Mode II characteristic length can be defined as follows:

$$l_{ch,II,slim} = \sqrt{E_{II,slim}\frac{G_{IIc}}{(T_S^o)^2}t} \tag{15}$$

In the case of a slim laminate, equation (13) should be reworked as follows:

$$E_{II,slim} = \frac{E_{11}}{1-\nu_{13}\nu_{31}} \tag{16}$$

Characteristic length can be plotted for different values of the critical energy release rate, for modes I and II, as shown in Figure 5.

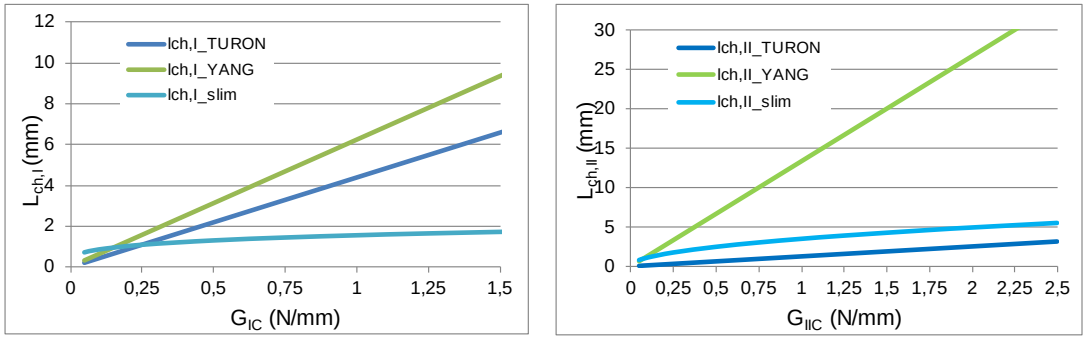

Figure 5. Characteristic length element according to the critical energy release rate.

With the exception of the formulae proposed by Turon, in the other two proposals (Yang and Cox, Bao and Suo) for the determination of the characteristic length of the CZM, the characteristic length values are greater for mode II than for mode I. Critical displacements due to mode II tend to be much higher than mode I. This usually happens when interlaminar friction is considered or interlaminar reinforcements through the thickness are included [13]. Therefore, whenever mode II is predominant, the use of the characteristic length as the reference length in order to create the mesh could lead to oversized mesh density. Taking all this into consideration, the use of the minimum length coming from the equation (17) is initially suggested. In addition, in order to obtain the optimum parameters, a parametric sensitivity analysis was also carried out.

$$L_{cz} = \min\left[L_{ch,i\_Turon}; L_{ch,i\_Yang}; L_{ch,i\_slim}\right]; \quad \text{con i} = \text{I, II} \tag{17}$$

Considering critical energy release rates between 0.45 and 1 N/mm for mode I and mode II shown in Figure 5, and applying equation (17), then a characteristic length equal to 1.219 mm can be obtained. This value can be calculated as well by using equation (14) based on Bao and Suo [39] formulae. This value is consistent with some authors' proposals [13], [34], [39], who stated that it is parameter-dependent on the material. Moreover, for polymeric reinforced composites L_{cz} is valued around 1.

The cohesive zone must be properly meshed around the tip of the crack. Low mesh density may lead to poor stress values in such an area. Therefore, a minimum number of elements along the cohesive zone should be arranged in order to achieve proper results by means of FEM. Many authors have conducted different studies in order to establish the minimum number of elements, obtaining diverging conclusions. Moës and Belytschko [40] suggested using more than 10 elements, Falk et al. [41] between 2 and 5. Davila and Camanho [21] considered that 3

elements are necessary to predict delamination evolution due to mode I, since this mode is the most restrictive in terms of minimum characteristic length. Not only were CZM used to predict delamination onset but they were also applied to determine its propagation. These studies were carried out on flat geometry specimens. This analysis was aimed at evaluating the minimum number of elements in the cohesive zone required to obtain reliable results. Moreover, the achievement of optimal computational costs was borne in mind for those specimens where delamination is linked to their curved geometry.

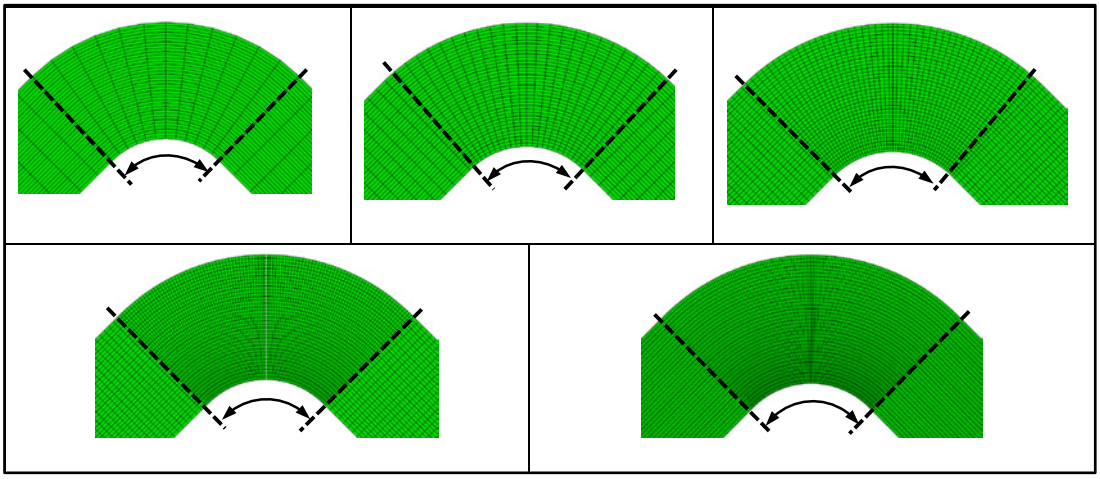

Figure 6. Effect of the element length.

With that purpose in mind, the 12-layer 2D model was used once more with 3 elements in the thickness of each layer. Additionally, the curved area was circumferentially discretized in a variable number of elements. More specifically, 12, 24, 48, 96 and 144 elements (Figure 6) were applied to the curved zone, by which, 1.3, 2.7, 5.3, 10.7 and 21.3 elements were respectively the corresponding elements modelling the characteristic length. Element size half-way through the thickness is shown in Table 3 for each model.

Table 3. Number of elements in the characteristic length of the cohesive zone.

Elements in curved zone	Element size half-way through the thickness (mm)	Elements in the characteristic length
12	1.484	1.3
24	0.742	2.7
48	0.371	5.3
96	0.185	10.7
144	0.093	21.3

If the results of the different simulations shown in Figure 7 are analyzed, it will be observed that the specimens modelled with 12 and 24 elements in the curved zone, corresponding to an element length of 1.484 and 0.742 mm, respectively, presents shows lower global stiffness in the elastic range. Besides, some discontinuities are appreciated in the load recovering stage after the first delamination. These discontinuities are directly related with the element length. For the rest of the models, the normalized load versus the applied displacement graphs shows strong correlation with the experimental results, both in terms of stiffness and yield load. Figure 7 (right) shows how the convergence increases as the number of elements on the curved zone rises. Although, the computational cost is initially reduced, it rises once more when the number of elements increases.

As a conclusion, it was stated that the optimum element length corresponds to a discretization with 48 elements in the curved zone, that is, 0.371 mm element length half-way through the thickness. This kind of model will be applied to the analysis of 8 and 12 layer models, whereas a 24 element discretization in the curved zone will be implemented for 4-layer models.

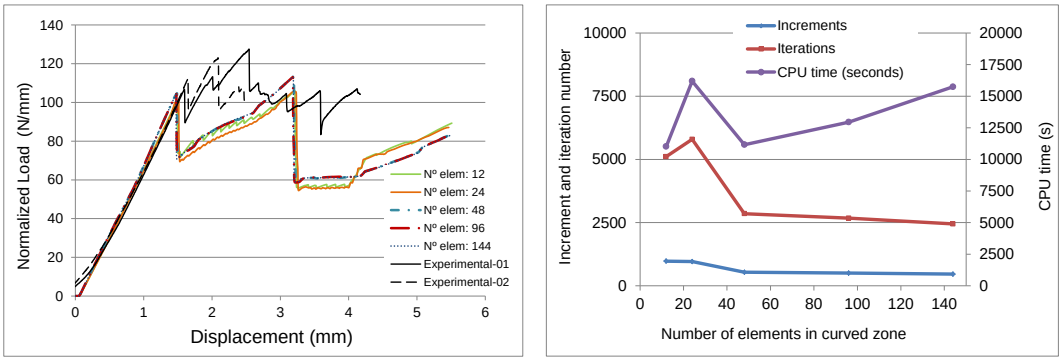

Figure 7. Influence of element numbers on the modelling curved zone: left) load-displacement curves; right) analysis performance.

4.3. Influence of the critical energy release rate

Critical energy release rates are determined experimentally through the Double Cantilever Beam (DCB) and End-Notched Flexure (ENF) tests, for mode I and mode II respectively. The energy rate related to mode III delamination is assumed to have a cohesive law equal to the rate for mode II, since there is no experimental information in the literature [13] and the few studies dealing with this mode of failure provide conflicting conclusions. For example, Krueger [12], from his experimental study, considers that the contribution of mode III to total fracture energy is negligible. However, Donaldson [42] presents numerical studies in which it is stated that delamination near notches or other discontinuities are completely addressed by the contribution of the stresses related with mode III. The justification for applying the same degradation laws to modes II and III, can be made from the physical point of view. In fact, the material in the crack progress zone turns out to be insensitive to the plane of the shear deformations to which is subjected [13].

Table 4 lists the most common values of critical energy release rates for unidirectional carbon / epoxy laminates from various sources. It can be seen that there are significant differences in these values. Therefore, the influence of the critical energy release rate in the four-point-bending test results is studied hereafter.

Table 4. Critical energy release rate for UD carbon/epoxy.

Author	G_{IC} (N/mm)	G_{IIC} (N/mm)
Mi & Crisfield [43]	0.514	1.014
Yang [13]	0.350	0.700
Liu [44]	0.252	0.665
Camanho [21]	0.268	N/A
Alfano & Crisfield [45]	0.330	0.800
Turon [1]	0.260	1.002
Song & Davila [34]	0.080	0.550

Firstly, a sensitivity analysis of the critical rate of energy release in mode I was carried out, by varying it in the range of values described by the different authors for this type of material, while

maintaining the rest of the initial parameters. Different normalized load vs displacement curves were obtained for different values of G_{IC} by means of the simulation of the ASTM D6415 test. It is possible to infer from Figure 8 (left) that an identical prediction of the rigidity and maximum load of ASTM D6415 test was obtained, and that the post-failure behaviour shows a lower load drop for higher G_{IC} values. In addition, there is not variation in the displacement at which the second load drop occurs, coinciding with the delamination of the second interface. Moreover, for the different critical energy release rates studied, no numerical problems of convergence arose.

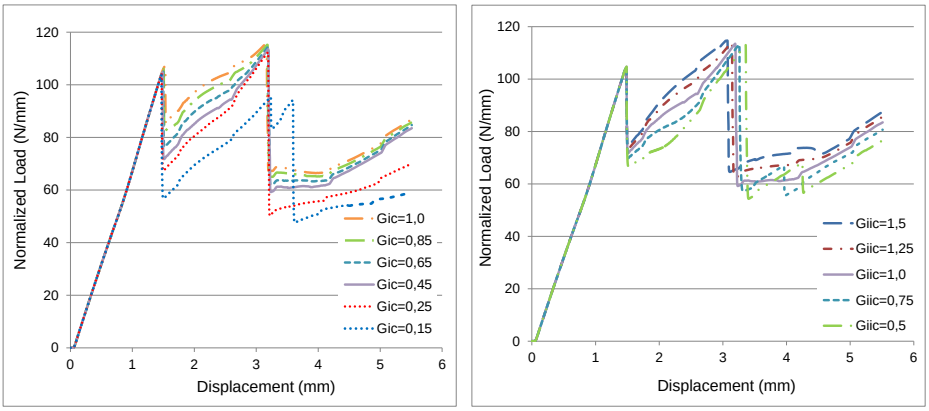

Figure 8. Influence of critical energy release rates: Mode I (Left) y Mode II (Right).

Subsequently, a sensitivity analysis of the critical rate of energy release in mode II was carried out, by varying it in the range between 0.5 and 1.5 N/mm, while keeping the rest of the initial parameters fixed and selecting a critical energy release rate for mode I equal to 0.45 N/mm. As before, there were no numerical convergence problems for the selected G_{IIC} range. Figure 8 (right) shows that, for the entire range of values, an identical prediction of the stiffness and the maximum load of the test were obtained. However, the sudden load drop in the post-failure behaviour, -once the maximum load has been reached- increases slightly as G_{IIC} decreases. Thus, G_{IIC} equal to 1 N/mm was selected. The validity of this selected parameter will be correlated with the corresponding experimental results in the following section.

5. Results and discussion

5.1. Bidimensional models

Figure 9 shows the numerical results obtained from the bilinear model by means of the previously selected discretization and parameters, for the 4, 8 and 12 layer unidirectional specimen models. As the normal interlaminar shear stress evolves, similar behaviour is observed in all the graphs of load against displacement. Initially, a linear evolution of load vs displacement is observed until the maximum load is reached. Immediately before reaching the maximum load, the safety coefficient in the interface reaches its maximum allowable value, defined by the quadratic failure criterion that was established for the cohesive elements. Therefore, the cohesive elements begin to degrade at that moment, according to the bilinear law defined for the model. The critical energy release rate is quickly reached, leading to the complete failure of the cohesive elements. The first delamination is then initiated, localized at 1/3 thickness from the inner radius (except for 4-layer coupons, where the first delamination happens between 1/2 and 1/3 of thickness), and all at once, a drop occurs in the normalized load to which the specimen is subjected. Subsequently, throughout the progress of delamination, a redistribution of stresses in the laminate takes place. Moreover, regions

separated by the delamination began to work independently, with the progressive increase of the separation between them. Nevertheless, the supported load progressively increases from that moment until it reaches another peak load. At that moment, the cohesive elements located between another pair of layers reach the maximum interface strength and begin to degrade, giving rise to a second delamination.

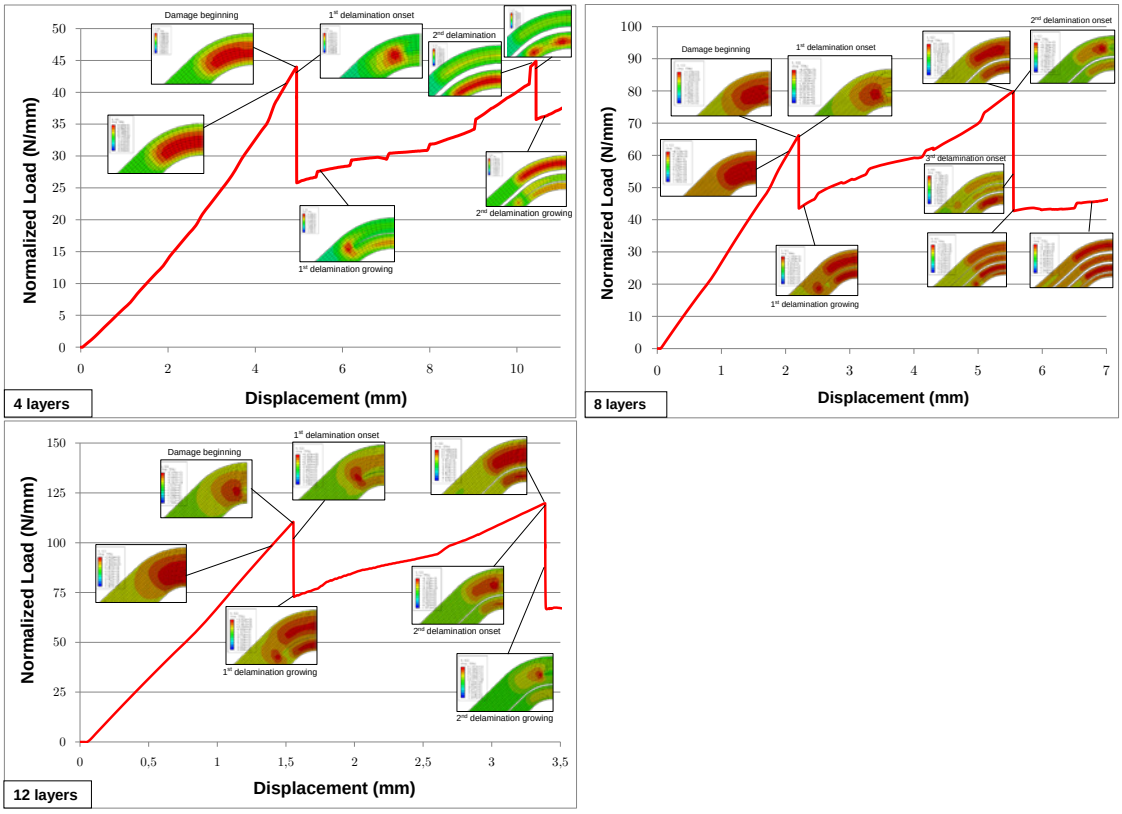

Figure 9. S_{33} distribution along the load-displacement graph. 4, 8 and 12 layer coupon.

Figure 10 depicts S_{33} stress distribution (interlaminar normal stress) and S_{11} (circumferential stress) through the thickness for the three different specimens (4, 8, and 12 layers) in the central position of the curved area (0º).

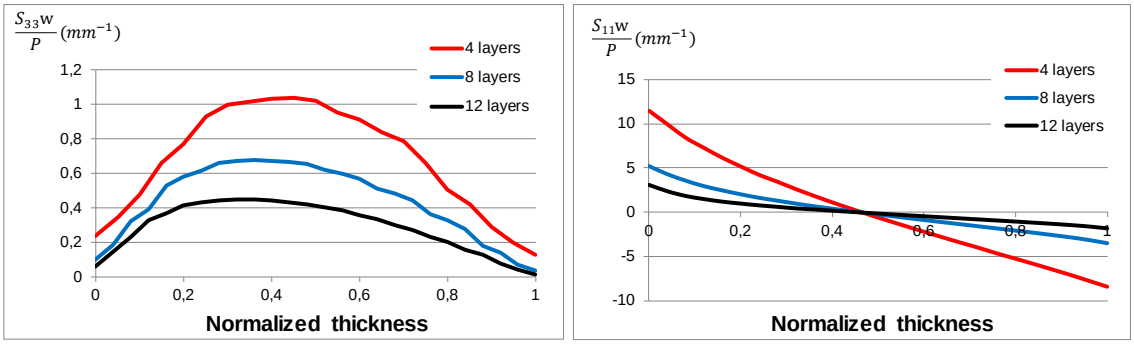

Figure 10. Influence of laminate thickness on stress distribution: left) S_{33}; right) S_{11}.

For a given load, it can be seen that the greater the thickness of the beam, the lower the values of interlaminar stress. It is also observed that the greater the specimen thickness is, the position

of the maximum interlaminar normal stress moves from the center to the inner radius. Additionally, the greater the thickness of the specimens, the lower the circumferential stress. However, the position where this circumferential stress becomes zero coincides with the center of the thickness and does not vary with the increase in thickness.

5.2. Numerical-experimental correlation

Figure 13 compares the results of bidimensional numerical models against those obtained experimentally by real tests. 4, 8 and 12-layer specimens were analyzed. The maximum strength reached for all numerical models was very close to those values obtained experimentally. Consequently, curved beam strength (CBS) and interlaminar tensile strength (ILTS), shown in Table 6 and Table 7, have small percentages of error in comparison with the experimental values. These CBS and ILTS values are calculated using the complete formulation of Lekhnitskii [46] by means of predictions obtained from the numerical models.

In terms of stiffness, finite element models show very strong correlation for 4 and 8 layer specimens. However, the 12-layer specimen shows a slight overestimation regarding stiffness. This deviation results from the fact that the scale effects are greater in those specimens with the highest thickness, with a higher number of defects. This is due to inadequate compaction achieved by means of the resin infusion technique [4] when the number of layers increases. These defects lead to a small decrease in the stiffness of the specimen when compared to the expected numerical calculation.

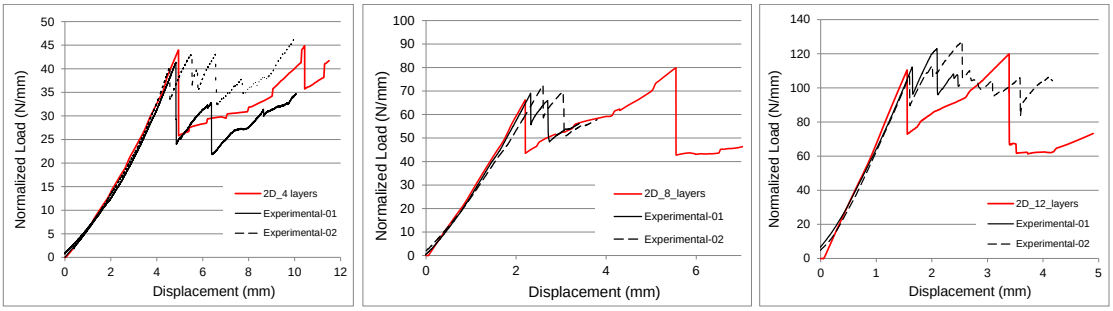

Figure 11. Comparison between load-displacement curves.

After the onset of the first delamination, a strong drop in the sustained load - greater than the one observed in the experimental curves - can be observed in all numerical models. Moreover, load recovery presents the same tendency in both numerical and experimental models. However, it can be noticed that the second and subsequent delaminations are predicted at much greater displacement in the case of the numerical models. Nevertheless, strong predictions of load level are achieved for this second delamination.

Table 5. Comparative of CBS (N).

	FEM 2D	Experimental[4]	Error 2D (%)
4 layers	1025	1002	2.30%
8 layers	1890	1944	-2.78%
12 layers	3152	3166	-0.44%

Table 6. Comparative ILTS (MPa).

	FEM 2D	Experimental[4]	Error 2D (%)
4 layers	48.87	51.76	-5.58%
8 layers	45.12	43.83	2.95%
12 layers	44.61	43.23	3.18%

6. Conclusions

A methodology has been proposed to predict the onset and evolution of delamination by means of a Cohesive Zone Model (CZM) with linear degradation throughout this study.
This methodology was applied to simulate the mechanical behaviour of curved specimens subjected to four-point-bending. The influence of different model parameters and the size element in the discretization was studied to determine the variation of the provided results.

Computational optimization for the developed models has also been sought, since the CZM establishes a characteristic length for the cohesive zone where delamination takes place. This characteristic length, together with the need to use the minimal number of elements in it to achieve good results, causes a large increase in the total number of elements in the models, having a negative impact in calculation times.

The proposed bilinear model has been applied on two-dimensional numerical models for different specimen thicknesses, providing very good results in terms of delamination onset prediction. With regard to the evolution of delamination, accurate prediction of the general trend is observed. However, in some aspects there are discrepancies between experimental and numerical results, such as the load drop after the first failure, or the displacement in which the subsequent delamination occurs. These issues can be improved in future models, by including considerations that have been ignored in this model.

All the problems of solid mechanics are rigorously three-dimensional; nevertheless, it has been established that for unidirectional laminates that do not present singularities in their geometry or effects of free edge, the simplification to two-dimensional models is justified. This claim is based on the good results obtained from the two-dimensional models. However, this is only applied to unidirectional laminates that do not present singularities in their geometry or free edge effects. The use of three-dimensional models, which involves an excessive computational cost, only makes sense for the analysis of singularities, such as holes, double curvatures or laminates with stiffness between layers of great difference. Sub-modelling strategies must be used for the study of these singularities found in certain technological applications. Moreover, cohesive elements should be restricted in sub-models due to the high mesh density imposed by the Cohesive Zone Model (CZM) methodology.

Data availability

The processed data required to reproduce these findings are available to download from https://doi.org/10.1016/j.compstruct.2016.12.010.

References

[1] W. Hao, D. Ge, Y. Ma, X. Yao, and Y. Shi, “Experimental investigation on deformation

and strength of carbon/epoxy laminated curved beams," *Polym. Test.*, vol. 31, no. 4, pp. 520–526, 2012.
[2] Raju, "Delamination damage analysis of curved composites subjected to compressive load using cohesive zone modelling," 2014.
[3] W. Cui, T. Liu, J. Len, and R. Ruo, "Interlaminar tensile strength (ILTS) measurement of woven glass/polyester laminates using four-point curved beam specimen," *Compos. Part A Appl. Sci. Manuf.*, vol. 27, no. 11, pp. 1097–1105, 1996.
[4] D. Ranz, J. Cuartero, A. Miravete, and R. Miralbes, "Experimental research into interlaminar tensile strength of carbon/epoxy laminated curved beams," *Compos. Struct.*, vol. 164, pp. 189–197, Mar. 2017.
[5] ASTM, "ASTM D6415/D6425M-06a Standard Test Method for Measuring the Curved Beam Strength of a Fiber-Reinforced Polymer Matrix Composite," *Annu. B. ASTM Stand.*, vol. 15.03, no. Reapproved 2013, pp. 1–10, 2015.
[6] S. C. Avalon and S. L. Donaldson, "Strength of composite angle brackets with multiple geometries and nanofiber-enhanced resins," *J. Compos. Mater.*, vol. 45, no. 9, pp. 1017–1030, 2011.
[7] R. Roos, G. Kress, M. Barbezat, and P. Ermanni, "Enhanced model for interlaminar normal stress in singly curved laminates," *Compos. Struct.*, vol. 80, no. 3, pp. 327–333, 2007.
[8] H. Ju, K.-H. Nguyen, S.-S. Chae, and J.-H. Kweon, "Delamination strength of composite curved beams reinforced by grooved stainless-steel Z-pins," *Compos. Struct.*, vol. 180, pp. 497–506, 2017.
[9] Z. Zou, S. R. Reid, P. D. Soden, and S. Li, "Mode separation of energy release rate for delamination in composite laminates using sublaminates," *Int. J. Solids Struct.*, vol. 38, no. 15, pp. 2597–2613, 2001.
[10] G. R. Irwin, "Analysis of Stresses and Strains Near the End of a Crack Traversing a Plate," *Appl. Mech. Div. Summer Conf. ASME*, pp. 361–364, 1957.
[11] M. A. Jiménez and A. Miravete, "Application of the finite-element method to predict the onset of delamination growth," *J. Compos. Mater.*, vol. 38, no. 15, pp. 1309–1335, 2004.
[12] R. Krueger, "Virtual crack closure technique: History, approach, and applications," *Appl. Mech. Rev.*, vol. 57, no. 2, p. 109, 2004.
[13] Q. Yang and B. Cox, "Cohesive models for damage evolution in laminated composites," *Int. J. Fract.*, vol. 133, no. 2, pp. 107–137, 2005.
[14] M. Elices, G. V. Guinea, J. Gómez, and J. Planas, "The cohesive zone model: Advantages, limitations and challenges," *Eng. Fract. Mech.*, vol. 69, no. 2, pp. 137–163, 2001.
[15] P. W. Harper and S. R. Hallett, "Cohesive zone length in numerical simulations of composite delamination," *Eng. Fract. Mech.*, vol. 75, no. 16, pp. 4774–4792, 2008.
[16] A. Turon, C. G. Dávila, P. P. Camanho, and J. Costa, "An Engineering Solution for using Coarse Meshes in the Simulation of Delamination With Cohesive Zone Models," *Nasa/Tm-2005-213547*, no. March, pp. 1–26, 2005.
[17] P. F. Liu, J. K. Chu, Y. L. Liu, and J. Y. Zheng, "A study on the failure mechanisms of carbon fiber/epoxy composite laminates using acoustic emission," *Mater. Des.*, vol. 37, pp. 228–235, May 2012.
[18] A. Needleman, "A Continuum Model for Void Nucleation by Inclusion Debonding," *J. Appl. Mech.*, vol. 54, no. 3, p. 525, Sep. 1987.
[19] © Dassault Systèmes, "Abaqus 6.11 Online Documentation." [Online]. Available: http://130.149.89.49:2080/v6.11/books/usb/default.htm?startat=pt04ch17s01aus101.html. [Accessed: 05-Apr-2019].
[20] G. Alfano, "On the influence of the shape of the interface law on the application of cohesive-zone models," *Compos. Sci. Technol.*, vol. 66, no. 6, pp. 723–730, 2006.
[21] P. P. Camanho and C. G. Dávila, "Mixed-Mode Decohesion Finite Elements for the Simulation of Delamination in Composite Materials," *Nasa/Tm-2002-211737*, p. 42, 2002.
[22] S. T. Pinho, L. Iannucci, and P. Robinson, "Formulation and implementation of decohesion elements in an explicit finite element code," *Compos. Part A Appl. Sci. Manuf.*, vol. 37, no. 5, pp. 778–789, 2006.
[23] A. Turon, C. G. Dávila, P. P. Camanho, and J. Costa, "An engineering solution for mesh

size effects in the simulation of delamination using cohesive zone models," *Eng. Fract. Mech.*, vol. 74, no. 10, pp. 1665–1682, 2007.
[24] Y. Lin, "Role of matrix resin in delamination onset and growth in composite laminates," *Compos. Sci. Technol.*, vol. 33, no. 4, pp. 257–277, 1988.
[25] J. C. Brewer and P. A. Lagace, "Quadratic Stress Criterion for Initiation of Delamination," *J. Compos. Mater.*, vol. 22, no. 12, pp. 1141–1155, 1988.
[26] M. Kenane and M. L. Benzeggagh, "Measurement of Mixed-Mode delamination Fracture Toughness of unidirectional Glass/Epoxy Composites With Mixed-Mode Bending Apparatus," *Compos. Sci. Technol.*, vol. 49, pp. 439–449, 1996.
[27] G. T. Camacho and M. Ortiz, "Computational modelling of impact damage in brittle materials," *Int. J. Solids Struct.*, vol. 33, no. 20–22, pp. 2899–2938, 1996.
[28] P. P. Camanho, C. G. Dávila, and M. F. De Moura, "Numerical simulation of mixed-mode progressive delamination in composite materials," *J. Compos. Mater.*, vol. 37, no. 16, pp. 1415–1438, 2003.
[29] S. Jacques, I. De Baere, and W. Van Paepegem, "Analysis of the Numerical and Geometrical Parameters Influencing the Simulation of Mode I and Mode II Delamination Growth in Unidirectional and Textile Composites," *Appl. Compos. Mater.*, vol. 22, no. 6, pp. 637–668, 2015.
[30] A. Turon, C. G. Dávila, P. P. Camanho, and J. Costa, "An Engineering Solution for Solving Mesh Size Effects in the Simulation of Delamination with Cohesive Zone Models," *Nasa Langley Res. Cent.*, vol. TM, no. June 2005, 2005.
[31] L. Daudeville, O. Allix, and P. Ladevèze, "Delamination analysis by damage mechanics: Some applications," *Compos. Eng.*, vol. 5, no. 1, pp. 17–24, 1995.
[32] Z. Zou, S. R. Reid, and S. Li, "A continuum damage model for delaminations in laminated composites," *J. Mech. Phys. Solids*, vol. 51, no. 2, pp. 333–356, 2003.
[33] T. Vandellos, C. Huchette, and N. Carrère, "Proposition of a framework for the development of a cohesive zone model adapted to Carbon-Fiber Reinforced Plastic laminated composites," *Compos. Struct.*, vol. 105, pp. 199–206, 2013.
[34] K. Song, C. G. Dávila, and C. A. Rose, "Guidelines and parameter selection for the simulation of progressive delamination," *2008 ABAQUS User's Conf.*, pp. 1–15, 2008.
[35] K. H. Nguyen, H. W. Ju, V. H. Truong, and J. H. Kweon, "Delamination analysis of multi-angle composite curved beams using an out-of-autoclave material," *Compos. Struct.*, vol. 183, no. 1, pp. 320–330, 2017.
[36] C. G. Hoover and Z. P. Bažant, "Cohesive crack, size effect, crack band and work-of-fracture models compared to comprehensive concrete fracture tests," *Int. J. Fract.*, vol. 187, no. 1, pp. 133–143, 2014.
[37] A. Hillerborg, "Analysis of crack formation and growth in concrete," *Cem. Concr. Res.*, vol. 6, pp. 773–782, 1976.
[38] J. R. Rice, "A Path Independent Integral and the Approximate Analysis of Strain Concentration by Notches and Cracks," *J. Appl. Mech.*, vol. 35, no. 2, p. 379, 1968.
[39] G. Bao and Z. Suo, "Remarks on Crack-Bridging Concepts," *Appl. Mech. Rev.*, vol. 45, no. 8, p. 355, 1992.
[40] N. Moes and B. Ted, "Extended finite element method for cohesive crack growth," *Eng. Fract. Mech.*, vol. 69, no. June, pp. 813–833, 2002.
[41] M. L. Falk, A. Needleman, and J. R. Rice, "A critical evaluation of cohesive zone models of dynamic fractur," *Le J. Phys. IV*, vol. 11, no. PR5, pp. Pr5-43-Pr5-50, 2007.
[42] S. L. Donaldson, "Mode III interlaminar fracture characterization of composite materials," *Compos. Sci. Technol.*, vol. 32, no. 3, pp. 225–249, 1988.
[43] M. Crisfield, "Progressive delamination using interface elements," *J. Compos. Mater.*, vol. 32, pp. 111–170, 1998.
[44] P. F. Liu, Y. H. Yang, Z. P. Gu, and J. Y. Zheng, "Finite Element Analysis of Progressive Failure and Strain Localization of Carbon Fiber/Epoxy Composite Laminates by ABAQUS," *Appl. Compos. Mater.*, vol. 22, no. 6, pp. 711–731, 2015.
[45] G. Alfano and M. A. Crisfield, "Finite element interface models for the delamination analysis of laminated composites: Mechanical and computational issues," *Int. J. Numer. Methods Eng.*, vol. 50, no. 7, pp. 1701–1736, 2001.
[46] S. G. Lekhnitskiy, *Anisotropic Plates*. 1969.